



High-Speed Videography of Welding — Part 1: Fundamentals

The selection of sensors, lenses, filters, and digital formats for maximum possible image resolution and capturing thermal radiation are discussed

BY S. D. GUEST, G. GÖTT, G. DAPP, J. CHAPUIS, AND P. F. MENDEZ

Abstract

This paper is the first of a three-part series comprehensively covering the field of high-speed videography in welding. This first part provides the fundamental concepts and resulting quantitative guidelines provided for minimum frame rates for several welding phenomena for maximum possible image resolution and the ability to capture thermal radiation from the welding process. Welding phenomena discussed include metal transfer, arc, and weld pool evolution with examples for gas metal arc welding (GMAW) and shielded metal arc welding (SMAW). The maximum possible image resolution for a given system is established based on the amount of time recorded, the buffer memory, the sensor resolution, the bit depth of the sensor, and the frame rate used. The application of Planck's radiation law indicates that emission at low temperatures can be undetectable. Quantitative guidelines are also provided for filter type and critical wavelengths associated with light emitted by plasmas of different welding processes and thermal emission from the hot metal. Digital sensors, lenses, optical filters, and digital formats for processing and distribution are treated in detail. The fundamentals reviewed in this paper, together with the practical implementations for front and back lighting (Part 2) and natural radiation lighting (Part 3), will provide welding researchers with a previously inexistent compilation of criteria to select proper equipment, accessories and parameters for high-speed imaging of a vast variety of phenomena in welding, laser welding, and associated processes, such as additive manufacturing or cutting.

Keywords

- Videography
- Lenses
- Filters
- Camera
- Wavelength
- High Speed

Introduction

The welding field has experienced a rapid transformation as high-frequency inverters and arc welding power supplies have enabled relatively inexpensive in-situ process control that was previously unavailable. These types of welding power supplies represent the vast majority of welding processes used worldwide and have stimulated research in metal transfer and arc stability optimization using microprocessor-controlled current and voltage waveforms.

The technique of choice for analyzing metal transfer in welding has been high-speed videography (HSV), often coupled with data acquisition. Modern digital cameras have enabled the massive use of HSV in corporate and academic research labs. Despite the extensive use of HSV for the analysis of welding, reports on its use tend to be problem-specific and seldom well documented (Refs. 1-19).

This paper aims to provide a broad survey of the HSV technique, specifically highlighting the different applications and methods used in welding literature. The authors' firsthand experience also informs the survey. Leading companies and training institutions use videos produced at the Canadian Centre for Welding and Joining that use the techniques described. A frequent question from users of these videos is how they are generated. Answering this question in a comprehensive and general way is the main motivation of this work.

Physical Features of Phenomena Observed

The welding arc is a plasma of ionized gas and metallic ions emitting ultraviolet, visible, and infrared radiation. The intensity and wavelength of emitted light are characteristics of the welding process, shielding gas composition, and arc current. Metals at high temperatures, whether solid or liquid, emit light across a broad spectrum.

The relative intensity of radiation from the molten metal droplets and weld pool is often lower than the arc light, making imaging difficult. The disparity in intensities is magnified when imaging processes with varying current levels, such as short-circuit or pulsed gas metal arc welding (GMAW). During short-circuit metal transfer, the arc is periodically extinguished during the droplet transfer period and immediately followed by the arc reignition and droplet formation periods. Pulsed free-flight metal transfer is characterized by relatively low background currents during the droplet formation period followed by a short-duration high current pulse that forcefully detaches the droplet.

In each metal transfer mode, the periods of high current overexpose the arc region and details of the metal transfer can be lost. Decreasing exposure retains detail during periods of high brightness; however, details in the lower intensity regions might not be visible. Modern cameras with logarithmic sensor response aim to address this challenge (Ref. 20). This extreme difference in light intensity within the same HSV observation is one of the greatest challenges to solve in any welding HSV activity.

Time Scales

Metal transfer in welding involves molten metal on a size scale such that capillary effects are dominant. The pressures involved in capillary phenomena, such as droplets, are of the order of $4\gamma/L$, where γ is the surface tension (of the order of 1.5 N/m for steel) and L is the characteristic size of the feature observed. The dynamic pressure resulting is $\rho L^2/(8t^2)$, where ρ is the density of the molten metal (of the order of 7000 kg/ m^3 for steel) and t is the timescale associated with the feature observed. The timescale resulting is of the order of

$$t = \sqrt{\frac{\rho L^3}{32\gamma}} \tag{1}$$

Considering a minimum of five frames within the timescale considered, an approximate recommendation for the minimum frame rate of capillary-driven phenomena is

suggested frame rate =
$$30\sqrt{\frac{\gamma}{\rho L^3}}$$
 (2)

where the frame rate is in fps, γ is in N/m, ρ is in kg/m³, and for this equation, L is in mm. Table 1 summarizes common welding events and suggested minimum frame rates for steel. The suggested frame rates for capillary phenomena are 25% higher for aluminum.

Table 1 — Summary of Common Welding Events and Suggested Minimum Frame Rates				
Event	Feature Size (mm)	Duration (ms)	Suggested Minimum Frame Rate (10³ fps)	
Short-Circuit Necking (Ref. 21)	0.5-3		3-40	
Globular Necking	0.5-3		3-40	
Globular Droplet Transfer	1–5	30	0.2	
Spray Droplet Detachment	0.2-2	0.5	10	
Spray/Pulsing Droplet Transfer	0.5-2	3	1.5	
Pulsing Necking Metal Droplet Oscillation	0.5-1.5		8–40	
Weld Pool Surface Movement	0.25-3	5	1	
Powder Consumable Tracking	0.1–1	1	5	
Anode/Cathode Spot		0.001	5000	
Spatter	0.1–2		1–5	

Emissions from Welding

From the point of view of high-speed videography of welding, there are three main sources of radiation: the molten metal (weld pool, electrode, powders), the plasma arc (in arc welding), and the beam (in laser processes).

Minor sources for emission or scattering include macroscopic particles, which range from condensing metal vapor (fumes) to small droplets. The fumes lead to radiation absorption and scattering, which can be challenging in videography. The same mechanism occurs in powder-based processes, where the particles can block the optical path to the region of interest.

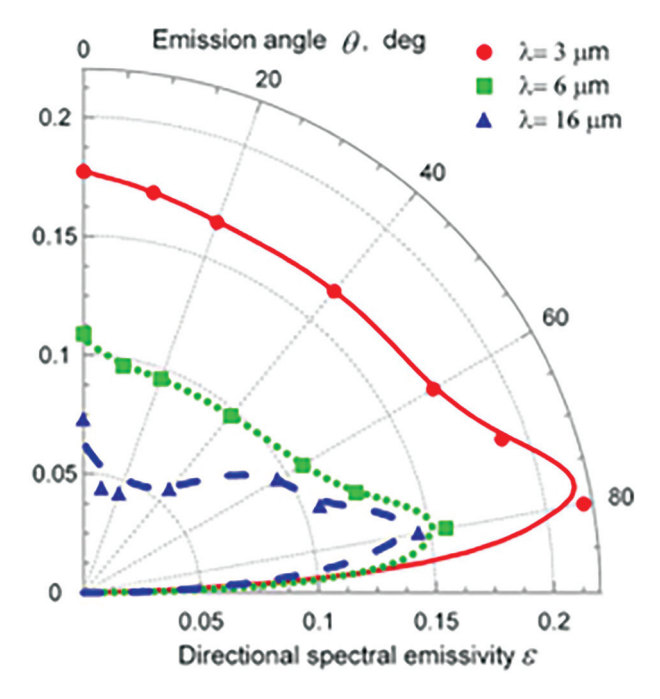


Fig. 1 — Directional spectral emissivity for metal at three wavelengths (Ref. 34).

Emissions from the Arc

In arc welding, the strongest radiation source is the arc itself. Light emission from the plasma is the consequence of the excitation of atomic and ionic energy levels by the high temperature of the arc. An important aspect of this excitation is that the bound electrons can only assume discrete energy levels, resulting in a quantization of the amount of energy released. Since the wavelength of radiation emitted is proportional to the energy of the electron jump (Ref. 22), the plasma light is emitted at particular wavelengths, not over a smooth spectrum. Although this reasoning would suggest that the plasma spectrum contains infinitely thin spectral lines, these lines are broadened by different effects related to the plasma parameters, such as temperature (Refs. 23-27).

From the point of view of imaging, understanding the wavelength of plasma emissions is important to identify constituents or to block plasma emissions. Table 2 lists wavelengths, including those of important gas and metal lines of elements introduced into the arc. These elements originate from the shielding gas and evaporate from the filler (of the electrode) and base material. Because plasma dissociates the molecules in the gas, the spectral response of an element is independent on the molecule it came from (e.g., oxygen coming from CO₂ in the shielding gas and O₃ from the electrode surface gives the same spectral lines).

Most elements in a welding arc have more than a few lines, making it difficult to define important lines without being misleading. For example, Fe has of the order 10³ lines in the visible range. Nevertheless, a useful heuristic is that metal lines tend to be below 600 nm whereas noble gases are found above 600 nm. Another useful heuristic is that the bright core in GMAW and other wire-based processes is usually associated with metal vapors.

In addition to transitions between energy states in bound electrons, there are also free-bound and free-free electron transitions. These free electrons lead to continuum background radiation.

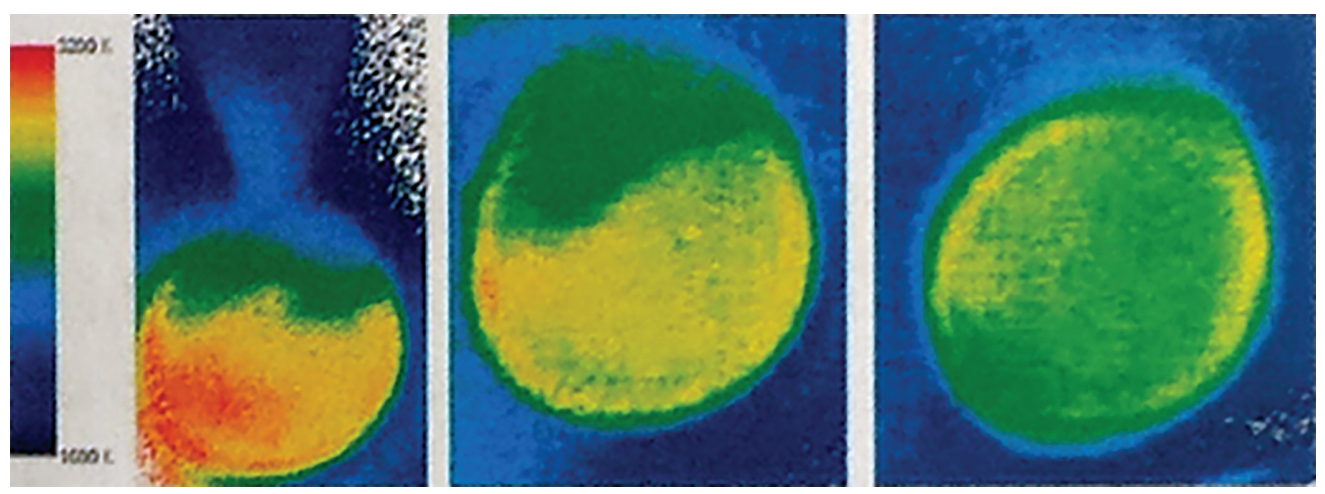


Fig. 2 — Surface temperature of a GMAW droplet, still attached to the wire, falling, and close to the weld pool (Ref. 35).

Table 2 — Important W	Vavelengths of Shieldi	ng Gas and Metal Vap	oor Spectral Lines and L	ight Sources
Gas/Light Source		Important Spec	tral Lines (nm)	
Arl	696	750	812	912
ArII	459	488		
He	921	952	1003	1091
CO ₂ /O ₂	777 (O I Triplet)			
H ₂	486	656		
Ca	526	559	616	
Mg	~ 382 (Triplet)	~ 45 (Triplet)	~ 518 (Triplet)	
Na	589			
Mn	449	600		
Fe	300-600			
Fiber Laser	1070 ± 5	1567 ± 2	532	
Disk Laser	1030	515 (green)		
Diode Laser	405	808	940-1060	
CO ₂ Laser	2000	9600	10,600	
Nd:YAG Laser	1064	946	1320	1444
Sodium Lamp	589			
LED	530	810	980	1050

Emissions from the Hot Metal

The second important radiation source in arc welding is the hot material in the welding area. The hot material is mostly molten metal but can also include oxides in oxidized places or in fluxes, silicates on the surface of the weld pool, and other components, such as tungsten carbide particles in some wear-resistant overlays.

In molten metals, the electrons are not in discrete states; therefore, they emit continuum radiation, which depends on the surface temperature and can be approximated as a "gray body" of emissivity $\epsilon <$ 1 (Refs. 28, 29). The wavelength at the peak of emission of thermal radiation is obtained from Wien's law

$$\lambda = \frac{2.898 \, 10^6}{T} \tag{3}$$

where λ (nm) is the peak wavelength of emission and T(K) is the temperature of interest. For 660°C (approximate melting temperature of aluminum) $\lambda = 3000$ nm, for 1500°C (approximate melting temperature of steel) $\lambda = 1600$ nm, and for 2500°C (approximate droplet temperature in GMAW), $\lambda =$ 1000 nm. Planck's distribution of radiation emission indicates that at a given temperature, emission decays at shorter wavelengths. This decay is gradual and allows us to see thermal emission even when the peak of emission is at wavelengths longer than the spectral response of the camera. However, the radiation emitted at low temperatures might be undetectable by a sensor. For example, a sensor with a dynamic range of 70 dB, in which the image does not saturate at 2500°C, 900 nm, will not detect thermal radiation below around 900°C. Shorter wavelengths will be undetectable at even higher temperatures. Reflected light (for example, from the arc) will still be captured regardless of the temperature of the surface.

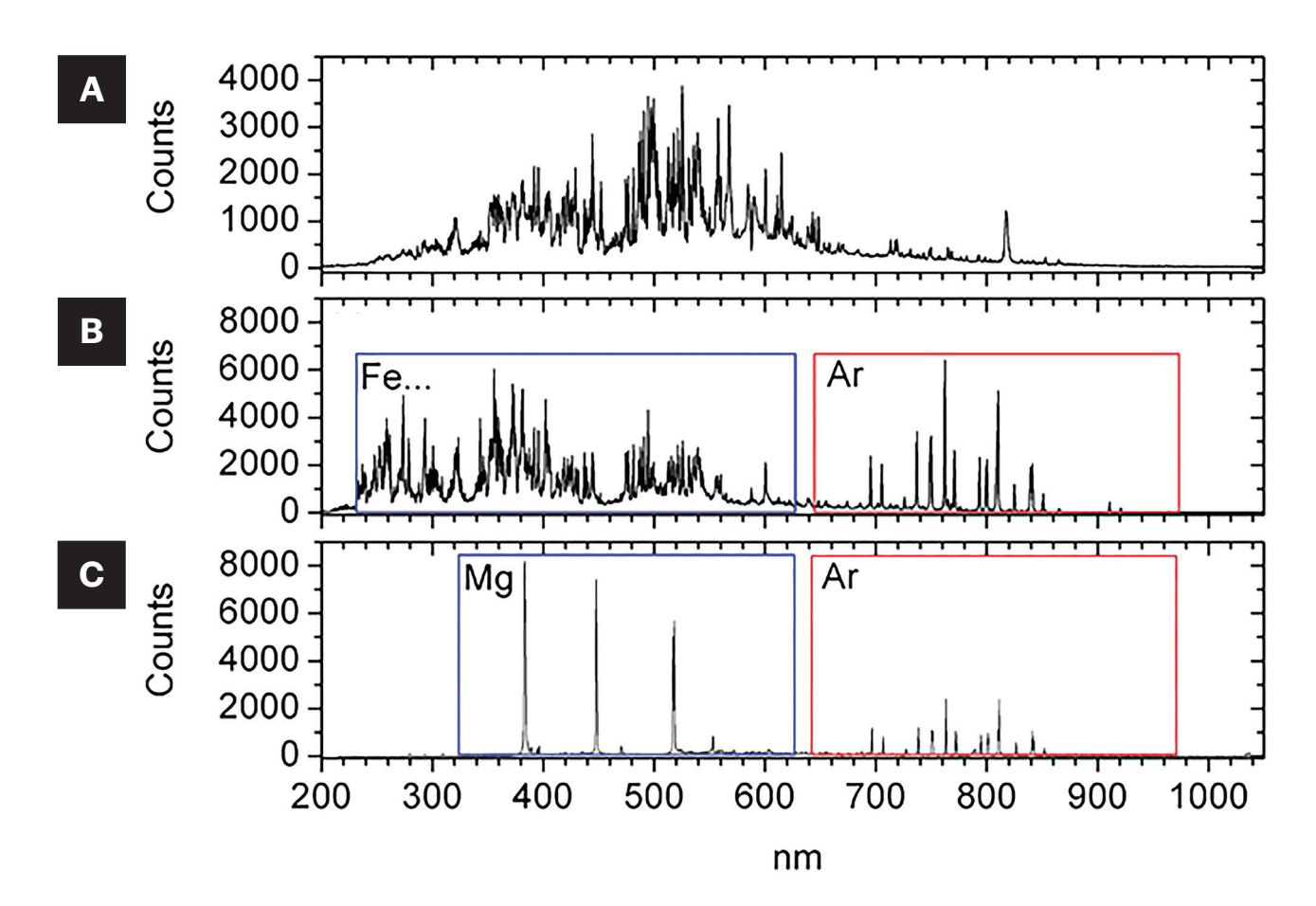


Fig. 3 — A — SMAW with a 7018 electrode; B — GMAW with a 1.2-mm ER70S-6 equivalent electrode in spray transfer mode with pure Ar shielding; C — GMAW with an ER5083 equivalent electrode with a pulse waveform and pure Ar shielding.

Oxides and other particles often do not behave like a gray body, with emissivity varying significantly with wavelength; however, their emissivity is typically higher than that of molten metal, and in consequence, they often look brighter, even when they are at the same temperature as the molten metal.

The emissivity for different materials at room temperature up to above the melting point can be found in Refs. 30-32. The emissivity of metals decreases sharply once metals melt because liquid metals have a highly reflective surface.

Another factor is the angular dependency of the emissivity of different materials, which is different for conductors and nonconductors. In (Ref. 33), a comparison between those two cases is demonstrated. The main difference is that nonconductors have an almost constant emission from 0-60 deg with only minor variation and are monotonically decreasing over the whole range. In contrast, conductors are fairly constant emitters too until 60 deg, but it is followed by a maximum between 70 and 80 deg.

The effect of the angle of emission should be considered when analyzing emitting surfaces and the measured intensity distributions, especially in welding. For simple imaging, the effect is of little significance; however, this effect is apparent under more sophisticated analysis. For example, Figure 3 shows thermal imaging of the droplet using two different wavelengths pixel-wise. Based on the assumption of a gray body, this method gets rid of the dependency on emissivity; however, the gray body hypothesis breaks down at angles of emission beyond 60 deg, resulting in erroneously higher temperatures assessed near the edges of the droplet.

Emissions from Lasers

In high-speed imaging of laser processes, the main challenge is ensuring that the wavelength of the laser is sufficiently blocked from the camera sensor to prevent overexposure or damage to the sensor. This can be achieved by using filters that are tailored to the wavelength that the laser is emitting. Such a "notch filter" blocks a great part of the radiation from the laser and can cost in the range of \$1000. For laser welding, it should have an optical density of 6 (transmissivity of 0.0001%). Even with such a filter, one should avoid damage to the camera sensor. In addition, due to the fast heating and cooling rates of laser processes, natural radiation is often too small for the camera to capture at high frame rates without an external light source.

Table 3 — Maximum Frame Rate and Frame Size of Selected High-Speed Cameras				
Frame Size (pixels)	Phantom V210 (2009) Maximum Frame Rate (binned output where available)	(fps)	Phantom VEO1310 (2020)	
1280 × 800	2190		12,906	
1280 × 720	2430		14,350	
960 × 960	4200		13,330	
640 × 480	6850		30,030 (40,300)	
480 × 480	7810		30,030 (40,300)	
320 × 240	20,600		57,360 (105,260)	
320 × 120			105,260 (180,680)	
256 × 128	50,000			
320 × 24			316,930 (423,350)	
128 × 32	200,000			
128 × 8	300,000			

Overall Spectra in Arc Welding

The complexity of the overall spectrum in arc welding was explored in (Ref. 36) by comparing the spectra of optical radiation from various welding arcs. Similar analysis of the arc spectrum is also presented in (Ref. 20). Figure 3 shows spectra for three kinds of welding arcs: SMAW with an E7018 electrode, GMAW with a G3Si1 electrode (roughly equivalent to ER70S-6) in spray transfer mode with pure Ar shielding, and GMAW of AlMg4.5Mn0.7 (aluminum consumable roughly equivalent to ER5083) with a pulse waveform and pure argon shielding. While Ar-CO₂ or pure CO₂ are more common shielding gases in GMAW of steels, the only noticeable spectral difference would be a weaker signal in Ar-lines. Otherwise, the spectra are almost identical since the C- and O-lines do not stand out at this resolution.

In the spectra of shielded metal arc welding (SMAW) and GMAW of steel, both radiation sources are visible, but the plasma radiation is still the most prominent. In the SMAW spectrum, the radiation from the evaporating steel and the electrode coating dominates the arc, evident in the peaks between 350–550 nm. In the GMAW of steel, the argon lines dominate (red box in Fig. 3) between 690 nm and 920 nm, whereas the metal lines are concentrated in the lower wavelength range below 640 nm (blue box in Fig. 3B).

In the spectrum of GMAW of aluminum, the same clear, sparse argon lines of spectrum 1b) are evident (red box in Fig. 3C) and a few lines from the evaporating magnesium are shown (see blue box in Fig. 3C). The absence of Al lines

is due to the preferential evaporation of magnesium, which has much higher evaporation pressure (Ref. 37). The fewer and more separated lines lead to no overlapping in the lines, which is present in spectra a) and b). In spectrum c), the influence of the black body radiation can be neglected, and it is not possible to see the radiation of the weld pool against the bright arc if the camera sensor is exposed to the whole visible spectrum.

The graphs of Fig. 3 are overall spectra of the arc; however, the arc itself can be subdivided into distinct regions that are clearly distinguished in their spectra. Arcs in GMAW with high Ar content have a characteristic structure with a brighter inner core that stands out from the surrounding plasma. Separate spectroscopy of the arc shows that the brighter core region is rich in metal lines, whereas the outer region emits mostly Ar lines. Research showed that the outer (darker) region is the one that is hotter and carries most of the arc current (Ref. 38).

High-Speed Videography Considerations

The rapid development of digital camera sensors with high data transfer rates has enabled high-speed cameras to become affordable while increasing the maximum frame rates and image resolutions.

For welding applications, the selection of parameters such as focal length and f-stop number depends not only on lens type and the area of interest but also on sensor type, sensor

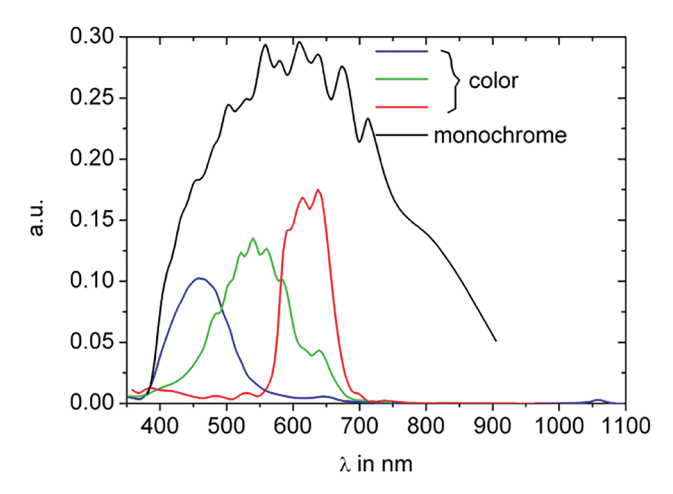


Fig. 4 — Spectral response as a function of photon wavelength for Phantom V210 camera sensor (blue, green, and red, labeled color) (Ref. 41) and IDT MotionPro Y4 (black, labeled monochrome) (Ref. 42).

sensitivity, frame rates, and the type of metal transfer. This results in many possible combinations that require careful consideration and selection by the videographer.

Sensors

Common digital camera sensors can be divided into two categories: charge-coupled device (CCD) and complementary metal-oxide semiconductor (CMOS). CCD sensors were the original type used in digital photography and videography and are commonly found in older generation cameras. Recently, CMOS sensors have become popular due to their low cost and low power consumption.

Exposure

Exposure is the time during which the sensor collects light. In modern cameras, this is controlled electronically. More-sensitive sensors require less exposure time to generate an equivalent image. In low-light conditions, longer exposure times can limit the maximum frame rate. Long exposure times relative to the time constant of the process observed might result in blurring.

In arc welding, higher currents result in a brighter arc, and when the current increases, keeping all other conditions the same, exposure should be reduced to maintain equivalent image quality. For example, in one experiment involving 1.6 mm Al E4043, exposure at 122 inches per minute (in./min, approximately 140 A) was 10 µs, but at 170 in./min (approximately 195 A), it was 5 μ s.

When data acquisition (e.g., current and voltage) is synchronized with the high-speed video, the data acquisition frequency is often much higher than the frame rate. The best estimate of data corresponding to a frame is the average collected data during exposure time.

Fill Factor

Fill factor is the ratio of the light-sensitive area of the pixel to the total pixel area. In CCD sensors, the sensor circuitry is below the pixel, enabling the entire sensor surface to collect light for a fill factor of 100%. In contrast, CMOS sensor circuitry occupies a portion of the pixel's light-collecting area, reducing the fill factor and decreasing the sensor's light-collecting ability. The decreased fill factor of CMOS sensors can be offset by small lenses placed over each pixel, collimating the light onto the light-sensitive pixel and away from the non-light-sensitive circuitry. The individual pixel circuitry of CMOS architecture increases the sensor's data transfer bandwidth and frame rate. CCD sensors do not have dedicated pixel circuitry, and the individual pixel information is transferred from the sensor in series, which reduces the sensor's data transfer bandwidth and maximum frame rate.

Shutter Mode

The entire sensor's pixel data must be transferred before another image can be taken. Circuitry considerations of the CMOS sensors have implications in the form of the sequence in which the obtained data is read out. This sequence is called the shutter mode (in an analogy to film photography). Most commonly, a sensor has a fixed shutter mode, with a few sensors offering multiple modes.

The global shutter mode in a CMOS sensor works similarly to a CCD sensor, and the integration of data of each pixel begins and ends at the same time. The rolling shutter, in turn, "sweeps" across the sensor and captures a sequence of pixel lines. This increases each pixel's duty cycle, reducing the delays between integration and readout. A rolling shutter allows higher frame rates but can cause motion blur where a moving object appears distorted, increased image noise at high gain levels, and can lead to artifacts in capturing pulsed light sources. The magnitude of these challenges increases with sensor size. Most high-speed video cameras provide some form of compensation through image processing.

Pixel Size

Larger pixels enable more light to be collected, increasing sensitivity. However, larger pixels decrease the image's resolution for a given sensor size. Under low or poor light conditions (e.g., natural light videography), a smaller sensor with smaller pixels produces lower quality images than a larger sensor with larger pixels. The primary driver for small pixels is lowering the sensor cost.

Larger pixel sizes are necessary to achieve the frame rates and sensitivity required for the short exposure times of highspeed videography. The sensor width-to-height ratio varies between manufacturers and does not follow the DSLR standards. Typical sensor sizes for high-speed video cameras are APS-C (approximately 350 mm²) and full-frame sizes (approximately 860 mm²). Smaller sensor sizes are available at a lower cost but are only capable of slower frame rates (Ref. 39). Sensor size also plays a role in the selection of lenses.

Subsampling

Subsampling (also known as windowing [Ref. 40] or "cropping") is a technique used to increase frame rates by reducing the number of active pixels at the expense of lower resolution. Subsampling is different from the "crop factor" that compares sensor sizes to full-frame sensors in photography and which has practical implications on magnification and field of view. Depending on the circuitry, cropping can take place in one direction or in both. Table 3 illustrates the size and maximum frame rate for two selected cameras.

An alternative to cropping is the combination of multiple pixels into a larger unit, known as "binning." This technology also offers increased frame rates at the expense of resolution. It was originally available in CCD sensors and only recently introduced to CMOS sensors. The advantage of this approach is a higher sensitivity and improved signal-to-noise ratio as the effective pixel size increases, as opposed to subsampling, where sensitivity remains the same.

Quantum Efficiency

Quantum efficiency describes the conversion efficiency of incoming light photons to electrons within the pixel. The conversion efficiency of pixels depends on the wavelength of incoming light, and this spectral response also depends on sensor design.

Figure 4 depicts the spectral response of one color and one monochromatic commercial sensor (Phantom V210 and IDT MotionPro® Y4). For the color camera, the higher color response with increasing wavelength is related to the increasing transparency of the color filters.

An interesting feature of the color camera sensor illustrated is some small sensitivity at 1050 nm (near-infrared region). This sensitivity to the near-IR of blue pixels is why images look blueish when using near-IR wavelengths, as seen in Refs. 32, 41–43, 45, and 47.

ISO Sensitivity

ISO sensitivity refers to the ISO 12232 standard *Photography – Digital still cameras – Determination of exposure index, ISO speed ratings, standard output sensitivity, and recommended exposure index* (Ref. 43), which applies to both monochrome and color camera sensors in the visible light spectrum. ISO sensitivity is a measure of sensor light sensitivity. A sensor with a higher ISO rating can provide more imaging options, including natural light videography or short exposure times for fast-moving features or high frame rates.

The determination of ISO sensitivity is typically performed by measuring the exposure time to sensor saturation and occasionally is determined from the minimum signal-to-noise ratio to create an acceptable image quality. The different methods can result in different sensitivities and image qualities. ISO sensitivity is affected by pixel size, fill factor, sensor filters, and quantum efficiency.

Both color and monochrome sensors are typically equipped with UV (< 400nm) and IR (> 700nm) filters to block the nonvisual wavelengths and preserve color rendering accuracy and image quality. For welding research applications where



Fig. 5 — Example configuration of 180-mm focal length lens (F-mount) with two 25-mm extension tubes, step-down rings, Φ 52-mm, 850-nm LWP filter, and Φ 52-mm UV filter for spatter protection. Some applications might benefit from a circular polarizer between the LWP and the UV filters.

sensitivity in the UV or near-IR is desired, these filters affect the consistency of commercial high-speed cameras over a broad spectral range. This inconsistency is often intensified by the camera's built-in image processor, making commercial high-speed cameras difficult to use as sensors for thermography or analysis of plasma spectral lines.

Color vs. Black and White Imaging

Camera sensors cannot distinguish between colors. Grayscale images result from the gradual saturation of pixels, with pure white corresponding to a fully saturated pixel.

For color imaging, filters are placed over the sensor to allow predetermined wavelengths of light to reach the pixel. The addition of color filters reproduces the perception of the human eye, and infrared filters eliminate the color distortion caused by infrared light.

Traditional (Bayer) filters on the sensor surface reduce the amount of light reaching the pixels and sensitivity. Modern strategies to overcome the loss of sensitivity include a micro-splitter approach that diffracts light, and different combinations of wavelengths reach different pixels (Ref. 44), gathering 1.85 times more light than traditional sensors. Another approach is the use of three-layer stacked sensors (Ref. 45), which have layered color-sensitive areas, such as US Patents US5965875, Color separation in an active pixel cell imaging array using a triple-well structure, and US6727521, Vertical color filter detector group and array. A trichroic beam-splitter or three separate sensors (Ref. 46) are modern technologies for color cameras but are not currently used for high-speed cameras.

Ultra-High-Speed Videography

The observation of phenomena such as cathode spots requires ultra-high-speed videography. Ultra-high-speed cameras (up to 10¹¹ fps) are usually equipped with an ICCD (intensified CCD) to increase light sensitivity due to the short

Table 4 — Overview of Common Mount Types, Flange Focal Distances, and Camera Type			
Mount	Flange Focal Distance (mm)	Camera Type	
C-Mount	17.526	Mirrorless, HSV	
D-Mount	12.29	Mirrorless	
Sony E-Mount	18	Mirrorless	
Canon EF-Mount	44	Mirror, HSV	
Nikon F-Mount	46.5	Mirror, HSV	
Arri PL-Mount	52	Professional moviemaking, HSV	

exposure time, and a beam-splitter (not spectrally selective) in which each optical channel is fitted with an individual ICCD. The ultra-high frame rates are achieved by triggering the ICCD successively. These systems are expensive and capture a relatively small number of frames, currently in the order of a maximum of 256 frames (Ref. 47). The image intensifiers can be tailored to a spectral range down to UV and up to IR.

Bit Depth

Bit depth describes the range of shades that a pixel can display. Typical camera sensors have 8 bits (256 shades) per color channel; this value is typically considered the minimum number of colors to perceive continuous color gradients. Modern high-speed cameras can have 12-bit sensors or higher. Higher bit-depths enable digital analysis of gradings that would not be possible with 8 bits, especially in regions of near extreme light or darkness, which are ubiquitous in welding videography.

Dynamic Range

Dynamic range is the range of exposure detected by the sensor from undetectable, minimum light intensity (pure black) to maximum light intensity causing sensor saturation (pure white). For commercial digital cameras, dynamic range is typically measured in dB (decibels) based on the maximum and minimum light intensity captured by the sensor:

dynamic range (dB) =
$$20 \log \left(\frac{\text{max light intensity}}{\text{min light intensity}} \right)$$
 (4)

For reference, the photo film used in old high-speed videography had a dynamic range of approximately 40 dB, and the human eye has a dynamic range around 50 dB (Ref. 48). Current digital sensors have a dynamic range comparable to film but better low-light sensitivity. The light emitted from the welding area involves radiation from plasma to radiation of metal below melting temperature, resulting in a range of intensities (and wavelengths) of the order of 70 dB, often exceeding the dynamic range of typical digital sensors.

The dynamic range of intensities in the welding region during arc welding also depends on time. A pulsed arc image typically varies its dynamic range from 10 dB to 80 dB. The emitted light also varies with the welding parameters. Short-circuit metal transfer brings the highest challenges to imaging because the bright arc is extinguished during the short-circuit stage and only light from the solid and liquid material is emitted. Camera sensors with the highest dynamic range are desirable for short-circuit transfer.

High Dynamic Range Processing (HDR)

The technique of HDR (high dynamic range processing) has not yet been implemented in research-level high-speed imaging of welding. Outside high-speed imaging, the HDR technique is seeing an increase in usage for process monitoring (Refs. 49, 50). There are two approaches to HDR imaging: one based on exposure settings and one based on sensor technology.

The exposure-based HDR technique works by compositing multiple exposures into a single frame that retains more detail in the bright highlights and dark shadows of the image. Mann et al. have developed a real-time 120 fps HDR imaging system for welding helmets (Ref. 51). This system combines four different exposures into a single frame, which can then be displayed to the welder via a screen inside the helmet. Recent developments in this area include the emergence of algorithms that use deep learning/neural network techniques to reduce the number of exposures necessary, increase speed, optimize the combination of frames into an HDR image, and reduce the number of artifacts (Ref. 52). The increased dynamic range can allow welders and operators to view the weld pool and the surrounding joint. The offline processing required to composite multiple exposures into a single frame over thousands of individual frames can be sufficiently large to require dedicated computers. Current high-speed cameras cannot change exposure between individual frames.

The sensor-based technology uses sensors with a non-linear response, typically logarithmic, to reduce oversaturation or a combined linear and logarithmic response to reduce image noise and artfacts (Refs. 39, 40). Non-linear behavior is also intrinsic to chemical films and the reason for their ability to capture difficult highlights in old welding videos. Another sensor-based approach to HDR is individual pixel control, in which a saturation threshold is set at the pixel level, stopping integration before saturation (Ref. 53) and retaining highlights of bright regions while maintaining a proper exposure in the darker regions of the image.

Memory Size

High-speed cameras temporarily store the video in a memory buffer. The size of this buffer's memory constrains the combination of maximum resolution, frame rate, and duration of phenomena observed. The maximum amount of real time observed can be estimated as

$$t = 8 \, 10^8 \frac{M}{H \, W \, D \, R} \tag{5}$$

where t (s) is the amount of real time recorded, M (GB) is the buffer memory, H and W are the sensor resolution in pixels, D is the bit depth in bits, and R (fps) is the frame rate.

For example, a camera with an 18 GB memory buffer can store approximately 39,000 frames at a resolution of 640 by 480 pixels of 12-bit depth. At 10,000 fps, this corresponds to 3.9 s of real-time video of welding phenomena. If the resolution was increased to 960 by 960 pixels, the amount of video would be reduced to 13,000 frames, or 1.3 s of real-time video at the same frame rate. Depending on the phenomena observed, the limiting factor can be memory size instead of resolution or frame rate.

Lenses

Focal Length

Focal length refers to the magnification or zoom of the lens. A longer focal length (e.g., 200 mm) results in a narrower field of view compared to a shorter focal length (e.g., 20 mm) lens, increasing the magnification of the image.

Reproduction Ratio

The reproduction ratio of the lens is the ratio of the object compared to the image to be formed on the sensor. A 5 mm feature appears as a 5 mm feature on the camera sensor with a reproduction ratio of 1:1, whereas the same feature appears as 2.5 mm on the sensor with a 1:2 ratio.

Aperture

Aperture represents the light-gathering ability of the lens, represented by the f-number. The f-number is inversely related to the diameter of the internal opening that allows light onto the sensor; a smaller f-number (e.g., f2.8) gathers more light than a larger f-number (e.g., f11).

Aperture variations are measured in terms of changes in the f-number, usually called f-stops, defined as

variation in exposure
$$(f - stops) = log_2 \left(\frac{light input 1}{light input 2} \right)$$
 (6)

such that when the light-gathering ability doubles, the f-stop is reduced by 1. Each f-stop decrease allows the exposure time to decrease by half, which is convenient for imaging fast-moving features in welding. The f-stop units can also be used for expressing dynamic ranges, in which one f-stop increase corresponds to a 6 dB increase.

Depth of Field

Depth of field, or the amount of the image in acceptable focus and clarity, depends on the reproduction ratio, focal length, minimum focus distance, and aperture. Larger apertures let increased light pass through while decreasing the depth of field. The bright light from the arc makes it amenable to use small apertures; however, apertures that are too small can result in increased diffraction and decreased image sharpness.

Magnification

Weld imaging often requires high magnification of the arc and weld pool zone. Typically, this can be accomplished with macro lenses, which are specially designed for detailed reproduction of small features (e.g., reproduction ratio near 1:1). A macro lens with a long focal length (e.g., 200 mm) keeps the front lens element/filters and camera body safely away from the welding heat and spatter. Such lenses are often expensive. Telephoto lenses with extension tubes can approximate the reproduction ratios of macro lenses, typically at much lower costs. The minimum focus distance of standard telephoto lenses affects the maximum reproduction ratio.

Long-distance microscopes can be used for the highest magnifications. This kind of lens has a working distance between 0.5 and 2.5 m. It works with a reflective optical system and has a field of view from a few millimeters to some cm, depending on the type and designer (Refs. 54, 55). It usually does not have an aperture, which is why a neutral density filter might have to be used to reduce the intensity of the arc.

Imaging Artifacts

Imaging welding operations also impose challenges on the lens. The bright welding arc can create chromatic aberrations and ghost surrounding objects of high contrast due to reflections within the lens. Chromatic aberrations can occur when collecting radiation with large differences in wavelength. Ghosting and flaring can occur from reflections between the last lens element and the sensor surface as well as from filters on the front lens mounts. High-quality lens manufacturers often coat lens elements to reduce chromatic aberrations, ghosting, and flaring.

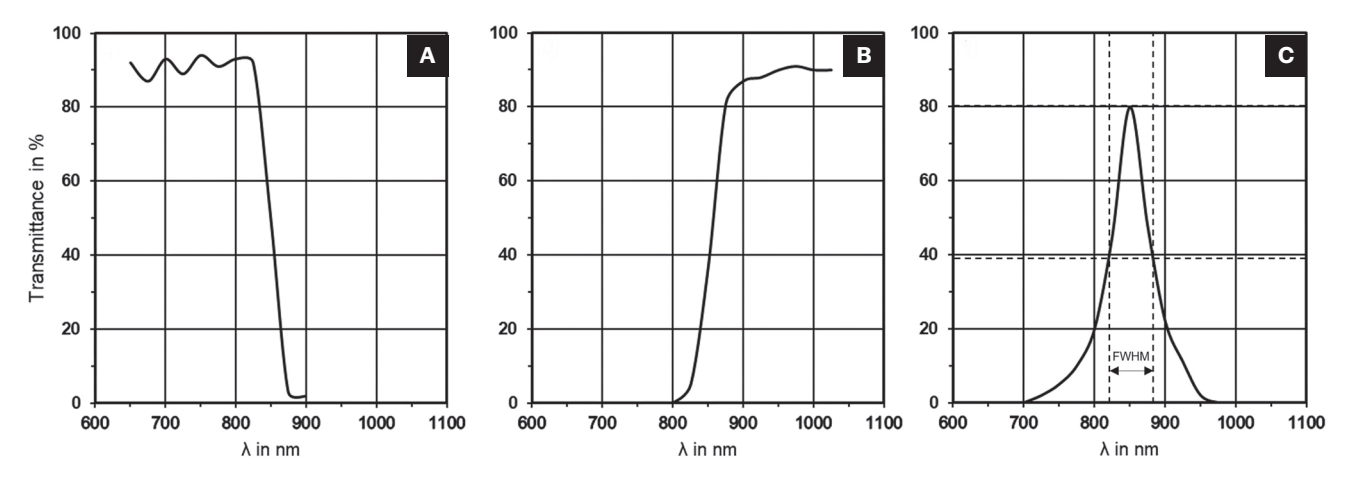


Fig. 6 — Spectral transmittance curves for 850 nm: A — SWP; B — LWP; C — BP filters.

Lens and Filter Mounts

Camera lenses are available in two mount styles: C-mount and bayonet mount. C-mount lenses mount to the camera body through a threaded mount and are common in machine vision or laboratory equipment. Bayonet mounts are common with consumer camera systems, such as DSLR cameras, where the ability to quickly interchange lenses is desired. These mounts are defined by the flange focal distance, which is the distance from the flange on the camera to the sensor surface, which is the minimum possible distance between the lens and the image sensor (Ref. 56). Common bayonet mounts are the Nikon F-mount and the Canon EF-mount lenses.

Camera lenses typically have threaded filter mounts in front of the front glass element. The filter mount diameter varies depending on the lens, and adapters (step-up or stepdown rings) can be used to mount filters to different lenses.

Transmission Spectrum

Photographic lenses are optimized for the visual range. Coatings reduce the spectral transparency to improve color rendering and sharpness. The glass itself is transparent between approximately 340 nm and 2000 nm. Specialized lenses for UV and IR are available but seldom used for welding research. The lenses themselves act as filters to be considered.

Filters

Filters pass and reject specific wavelengths of light; wellknown filters for welding are used in welding helmets, specified in ISEA Z87.1, American National Standard for occupational and educational personal eye and face protection devices (Ref. 57). Filters commonly used in welding videography include neutral density (ND), short wave pass (SWP), long wave pass (LWP), band pass (BP), and narrow band pass (NBP). A notch or band rejection filter is commonly used for laser applications.

Filter Technology

Filter technology attenuates incoming light through reflection or absorption. Interference or dichroic filters have a thin metal coating that combines absorption and reflection to filter the incoming light; the reflectivity of these filters can produce ghosting from internal lens reflections. Absorption or all-dielectric style filters absorb all the undesired wavelengths within the filter while passing the wavelengths of interest. Absorption-style filters reduce reflections and scattered light and are preferable.

Neutral Density Filters

Neutral density filters, sometimes called gray filters, reduce light intensity by approximately the same amount in all wavelengths of interest. Generic ND filters are typically manufactured to reduce the intensity of visible light for commercial and entertainment videography work. Some ND filters provide no attenuation of UV or near-IR radiation, an important consideration for welding, where there is strong emission in both UV and IR wavelengths. ND filters are often specified by their reduction in transmittance through either optical density or equivalent f-stops.

Edge Filters (SWP and LWP)

Edge filters, which include short wave pass and long wave pass filters, selectively block or pass desired wavelengths of light above or below a specified wavelength. Edge filters typically use interference effects rather than absorption, creating a steep transition between blocked and transmitted light.

A SWP filter allows all light with shorter wavelengths than specified to pass through while blocking longer wavelengths, as shown in Fig. 6A. This type of filter would be useful, for example, to analyze the arc without interference from the IR radiation from the molten metal.

LWP filters transmit longer wavelengths, as shown in Fig. 6B. This filter can block the UV from the arc and capture the visible and infrared radiation; thus, it is ideally suited to study metal transfer phenomena.

Table 5 — Common Frame Sizes (Refs. 71, 74–77)

Name	X-Axis Resolution	Y-Axis Resolution	Frame Ratio (x:y)	Megapixels
PAL (analog)	720*	576	59:54 and 118:81*	~ 0.4
NTSC (analog)	720*	480	10:11 and 40:33*	~ 0.35
DVD	720	576/480	4:3	0.415/0.346
XGA	1024	768	4:3	0.786
720p (HD Ready)	1280	720	16:9	0.922
1080i/p (Full HD)	1920	1080	16:9	2.074
1440p (Quad HD)	2560	1440	16:9	3.686
2160p (4K UHD)	3840	2160	16:9	8.294
4320p (8K UHD)	7680	4320	16:9	33.178

^{*}The analog nature of these formats results in an ill-defined x-axis resolution, given here as an approximation.

SWP and LWP filters are useful for collecting light ranges, including metal and shielding gas spectral peaks in the same image. The wide range of light transmitted in edge filters can gather a greater intensity of welding radiation, making higher frame rates and lower exposure times possible.

The broad range of collected radiation can pose problems when the camera's dynamic range is limited, potentially oversaturating the image in some regions of high intensity due to specific spectral peaks from the arc (e.g., Fe lines at 200-600 nm).

Band Pass Filters

Band pass filters isolate specific light wavelengths while blocking shorter and longer wavelengths, as shown in Fig. 6C. BP filter transmission ranges can be wide or narrow, depending on the range of study. Combining two edge filters can effectively create a band pass filter in which light between two wavelengths is transmitted while all others are blocked by the SWP and LWP filters.

The width of the spectrum transmitted in BP filters is typically qualified by its full-width-half-maximum (FWHM) value. For example, the FWHM of the BP filter of Fig. 6C is 70 nm.

Narrow Band Pass Filters

Narrow band pass filters are a subset of band pass filters in which the range of wavelengths transmitted is narrow (FWHM < 10 nm). Producing NBP filters with a narrow transmittance profile is difficult and costly.

NBP filters are an important tool for imaging specific spectral peaks from the arc, such as metal vapor or argon lines,

where the spatial distribution of elements and temperatures can be determined (Refs. 38, 58-62).

Using the frontlighting or backlighting imaging techniques described in Part 2, an NBP filter can attenuate unwanted arc and metal light while capturing the light source wavelength. The specific filtering greatly improves the lighting source's efficiency and image quality.

Band Rejection Filters

Band rejection or notch filters have the inverse function of NBP filters and have one or multiple narrow attenuation bands. Like NBP filters, their production is difficult and costly. In laser applications, these filters selectively block the wavelength of the laser and can help mitigate damage to the sensor.

Considerations for Dissemination of **High-Speed Videos**

High-speed videos typically result in large files, of the order of 2 GB and larger, often in a proprietary file format specific to the camera manufacturer. Important aspects to consider for dissemination are the choice of playback frame rate, compression algorithms (codecs), file containers, and upscaling and downscaling techniques.

Playback Frame Rate

Typical playback video frame rates range from 24 fps to 30 fps. Frame rates greater than 60 fps require special fast decoding or decompressing and can cause problems with current hardware and video players.

Scenario	Equipment	Backlight	Lighting Setup Front Light	Natural Light
		Visible (400–700 nm)	Visible and near IR (400–1000 nm)	
	Camera sensor sensitivity		Monochrome: optimal	
General	General Monochrome/color camera		Color: feasibility depending on spectral response	Visible and near-IR (400–1000 nm)
Lens		200-mm f2.8 macro lens or 100– 200-mm f2.8 lens with 20–50-mm extension tubes		
Metal		20-mW laser with 650-nm	> 100-W laser with 800- 950-nm wavelength NBP \pm 5 nm centered on	N/A
Transfer		NBP 650 nm +	laser wavelength	> 850 nm LWP
Frame rates	5 nm	General investigations: 5000 fps Scientific analysis: 10,000-30,000 fps		
				N/A
Arc	Supplementary light source	N/A	N/A	< 600 nm for meta vapor; 700 nm for Ar; 777 nm for O
	Filter	IV/A	IV/A	10,000-50,000 fps
	Frame rates			(~ 1,000,000 fps for cathode spot movements)

Excessive capture frame rates might result in unnecessarily long videos. Because playback speed is limited, accelerating playback might require eliminating frames or using interpolation techniques.

Codec

The codec is the compression/decompression algorithm used to store and play the videos taken. Different codecs offer different levels of compression, from lossless to high compression.

Compression codecs use mathematical techniques based on spatial and temporal redundancies and changes. Codecs also exploit perceptual features of human vision, such as being more sensitive to changes in brightness than in color in neighboring pixels.

The MPEG-2 codec is among the oldest codecs, originally used in mass-market digital video distribution as DVDs. Newer codecs with improved compression algorithms produce higher resolution images with smaller files but require higher computational and hardware resources.

Modern codecs such as MPEG-4 AVC (Advanced Video Coding) and H.264 codec (defined under ISO/IEC 14496,

Information technology – Coding of audio-visual objects [Ref. 63]) exist in various proprietary and open-source implementations (e.g., x264). These codecs are lossy (some details are lost during encoding) and offer a range of compression levels.

The optimal compression and file size combination depends on the application, such as the maximum allowable size for supplementary material in peer-reviewed journals. New codecs like HEVC (defined under ISO/IEC 23008-2, Information technology – High efficiency coding and media delivery in heterogeneous environments, MPEG-H Part 2: High efficiency video coding [Ref. 64] and ITU-T H.265, High efficiency video coding [Ref. 65]), VVC (defined under ITU-T Recommendation H.266, Versatile Video Coding, and ISO/ IEC 23090-3.VVC, Information technology - Coded representation of immersive media, Part 3: Versatile video coding [Ref. 66]), and royalty-free codecs VP8 Data Format and decoding Guide (Ref. 67), VP9 Bitstream & Decoding Process Specification v0.6 (Ref. 68), and AV1 Bitstream & Decoding Process Specification (Ref. 69), can provide even higher compression rates with video qualities comparable to MPEG-4 but have higher hardware and computational requirements. Most web browsers have built-in support for MP4, VP8, and VP9, which eliminates the need for external players, and hardware

acceleration for these codecs exists in some modern GPUs, Smart TVs, and smartphones.

Modern codecs can present compatibility challenges for presentation software, such as Microsoft PowerPoint; in these cases, the slightly less-efficient MPEG-4 ASP (Advanced Simple Profile) codec can be used, available in various commercial and open-source implementations (e.g., x264, QuickTime 7). CCWJ videos are typically encoded as MP4 or VP8 for maximum compatibility.

Container

The container or wrapper format is a metafile format whose specification describes how different data elements and metadata coexist in a computer file; for example, the method with which audio and video data are contained and played back simultaneously. Data types can include multiple individual audio and video streams, metadata or tags, logos, watermarks, text, and subtitles.

The most popular container formats are the .avi format, .mp4 (which may also appear as .m4v), the royalty-free .webm format, and the open-source .mkv format. Other proprietary container implementations include 3GP (.3gp), QuickTime (.mov or .qt), Real Media (.rmvb), or Flash (.flv).

It is convenient to choose a container with maximum device, operating system, and software compatibility for various usages, such as the .mp4 container. If the primary purpose is online streaming, .mp4 or .webm containers may best suit current web browsers.

Frame Size

As a result of subsampling, the frame sizes of high-speed videos are often non-standard. Several standards define common sizes for various organizations, applications, and purposes, such as ATSC A72 Part 1(Ref. 70), DVB ETSI TS 101 154 V2.6.1, Digital video broadcasting (DVB); specification for the use of video and audio coding in broadcast and broadband applications (Ref. 71), ITU R BT.2020-2, Parameter values for ultra-high definition television systems for production and international programme exchange (Ref. 72), DCI Digital Cinema System Specification v. 1.3 (Ref. 73), and SMPTE ST2036-1, SMPTE standard – Ultra high definition television – Image parameter values for program production (Ref. 74). Common frame sizes are listed in Table 5.

Any resolution above XGA is currently called "high definition." Naming conventions often fulfill a marketing function. Standard frame sizes for distribution of high-speed videos include HD 1280 \times 720 pixels and Full HD 1920 \times 1080 pixels. With a new generation of sensors, UHD resolutions will likely become more common.

Standard frame sizes are important for built-in acceleration algorithms in the CPU or GPU to encode or decode high-resolution images using high-efficiency codecs. Codecs and containers are optimized for standard resolutions and aspect ratios, and non-standard parameters can result in videos of inferior quality. For example, the low pixel count commonly used in high-speed videography might not provide the decompression algorithm with sufficient information to produce high-quality images. This often results in grainy and

low clarity images, even when the information contained in the file corresponds to higher quality video. Current software included with high-speed video cameras (e.g., PCC for Phantom cameras [Ref. 78]) has built-in compression capabilities; however, the software is optimized to control the cameras and obtain the basic video data, and the best results involve post-processing with additional specialized software tools.

Frame Size Editing

Upscaling, or interpolating, the image to a standard frame size for distribution helps overcome the limitations of codecs and software to decompress non-standard sizes. To achieve a standard aspect ratio, borders can be added to the image's top, bottom, or sides to fill in the missing areas of the frame. If solid color borders are used, they add negligible information and do not increase file size.

Numerous commercial (e.g., Adobe Premiere [Ref. 79], Lightworks [Ref. 80], Final Cut Pro [Ref. 81], and DaVinci Resolve [Ref. 82]) and open source software (e.g., Kdenlive [Ref. 83], OpenShot [Ref. 84], Avidemux [Ref. 85], and HandBrake [Ref. 86]) solutions are available to apply, convert, or adjust codec settings during or after video editing. Most video editing software allows for various codecs and settings, although the selection available often depends on commercial considerations. Open-source software often allows for the greatest flexibility but has only limited access to commercial codecs.

File Size

Compressed video size depends on the number of changes that occur in the state of individual pixels in a series of digital images. A practical consequence of this is that capturing footage of a pulsed or short-circuit welding process that contains periods of relative inactivity ("darkness") produces smaller files than a process with more visual activity (e.g., high-speed videography of submerged arc welding).

The interrelation of visual activity, compression, and image quality means no setting will be optimal for all scenarios. A two-step process can reduce the complexity of selecting compression settings to achieve an acceptable balance of image quality, file size, and ease of use.

In the first step, a first level of compression (approximately a factor of 20 to 40 using camera-specific software) in the rendering stage of video editing reduces the file size of the uncompressed files (~ 2 to 4 GB) to 50–200 MB while retaining a high image quality. In the second step, these files are then compressed again using specialized video editing software (e.g., HandBrake) and customized presets to further reduce file size while optimizing the balance of file size and quality based on the intended purpose (e.g., email, presentations, journal submission).

Conclusions

The foundations of high-speed videography of welding phenomena are provided in detail. Quantitative guidelines are provided for minimum frame rates for several welding

phenomena, maximum possible image resolution, and the ability to capture thermal radiation.

Welding phenomena discussed include metal transfer, arc, and weld pool evolution. Recommended typical frame rates range from 1000 to 10,000 fps, although special situations might be outside this range. The maximum possible image resolution for a given system is established based on the amount of time recorded, the buffer memory, the sensor resolution, the bit depth of the sensor, and the frame rate used. Planck's radiation law indicates that emission at low temperatures can be undetectable. For a typical sensor dynamic range of 70 dB, if the image does not saturate at 2500°C, 900 nm thermal radiation will be undetectable below 900°C.

Guidelines are also provided for filter type and critical wavelengths associated with light emitted by plasmas of different welding processes and thermal emission from the hot metal; in particular, the discrimination of shielding gas and metal vapors is possible. Metal lines tend to be in the range below 600 nm, whereas the lines of noble gases are above 600 nm. Digital sensors, lenses, optical filters, and digital formats for processing and distribution are discussed in detail.

The fundamentals reviewed in this paper, together with the practical implementations for front and back lighting (Part 2) and natural radiation lighting (Part 3), provide welding researchers with a previously inexistent compilation of criteria to select proper equipment, accessories, and parameters for high-speed imaging of a vast variety of phenomena in welding and associated processes.

Appendix

Acronyms

BP	Band pass
BR	Band rejection
CCD	Charge coupled device
DSLR	Digital single lens reflex
fps	Frames per second
FWHM	Full width half maximum
GPU	Graphics processing unit
HDR	High dynamic range processing
HSV	High-speed videography
ICCD	Intensified charge coupled device
IR	Infrared
LWIR	Long wavelength IR
LWP	Long wave pass
NBP	Narrow band pass
ND	Neutral Density
RGB	Red, green, and blue color channels
SWIR	Short wavelength IR
SWP	Short wave Pass
UV	Ultraviolet

Dand sacc

Acknowledgments

The authors gratefully acknowledge support from the Natural Sciences and Engineering Research Council of Canada (NSERC), Prairies Economic Development Canada (Prairies-Can), and CWB Welding Foundation. The authors also thank the Leibniz Institute for Plasma Science and Technology in Greifswald, Germany. Productive conversations with and expertise from Eduardo Alvarez Rocha, Dr. Ivan Pigozzo, Carter Trautmann, and Daniele Calista, along with editing help from Jay Kahar and Aaryan Kumar, are also acknowledged.

References

- 1. Lu, Y., Chen, S., Shi, Y., Li, X., Chen, J., Kvidahl, L., and Zhang, Y. M. 2013. Double-electrode arc welding process: Principle, variants, control and developments. Journal of Manufacturing Processes. DOI: 10.1016/j.jmapro.2013.08.003
- 2. Norrish, J., and Cuiuri, D. 2013. The controlled short circuit GMAW process: A tutorial. Journal of Manufacturing Processes. DOI: 10.1016/j.jmapro.2013.08.006
- 3. Wang, Z. Z., Yu, Y., Chen, S. J., and Zhang, Y. M. 2012. Droplet tracking in double-electrode GMAW. Advanced Materials Research 418-420: 1180-1183. DOI: 10.4028/www.scientific.net/AMR.418-
- 4. Wang, Y. 2012. Research on lagging melt phenomenon and influencing factors of flux cored arc welding. Advanced Materials Research 557-559: 1326-1329. DOI: 10.4028/www.scientific.net/
- 5. Mistodie, L. R., Rusu, C. C., and Scutelnicu, E. 2011. Influence of pulsed gas metal arc welding parameters on the electric arc and droplet geometry. Welding Equipment and Technology 22: 62.
- 6. Zheng, S., and Gao, H. 2011. Experimental study on GMAW with strip electrode. Advanced Materials Research 314-316: 1025-1028. DOI: 10.4028/www.scientific.net/AMR.314-316.1025
- 7. Lee, K.-B., Kim, C., and Kim, D.-S. 2013. High deposition rate pulse gas metal arc welding for Al 5083 thick plate. Proceedings of Institution of Mechanical Engineers Part B Journal of Engineering Manufacturing 227: 848-854. DOI: 10.1177/0954405413476860
- 8. Ni, J., and Gao, H. M. 2013. Influence of preheated wire on GMAW process. Advanced Materials Research 668: 538-542. DOI: 10.4028/ www.scientific.net/AMR.668.538
- 9. Zhang, C., Li, G., Gao, M., Yan, J., and Zeng, X. Y. 2013. Microstructure and process characterization of laser-cold metal transfer hybrid welding of AA6061 aluminum alloy. The International Journal of Advanced Manufacturing Technology 68: 1253-1260. DOI: 10.1007/s00170-013-4916-y
- 10. Liu, A., Tang, X., and Lu, F. 2013. Weld pool profile characteristics of Al alloy in double-pulsed GMAW. The International Journal of Advanced Manufacturing Technology 68: 2015–2023. DOI: 10.1007/ s00170-013-4808-1
- 11. Zhang, Z. D., and Cao, Q. J. 2012. Study on metal transfer behaviour in metal inert gas arc welding with activating flux for magnesium alloy. Science and Technology of Welding & Joining 17: 550-555. DOI: 10.1179/1362171812Y.0000000046
- 12. Zhang, Z. D., and Kong, X. Y. 2011. Study on DC double pulse MIG welding of automobile aluminum alloy. Advanced Materials Research 295-297: 1933-1937. DOI: 10.4028/www.scientific.net/ AMR.295-297.1933
- 13. Yin, F., Zhu, S., Liu, J., and Wang, Q. W. 2011. Study on the incline limit in gas metal arc welding based rapid forming. Advanced Materials Research 189–193: 766–770. DOI: 10.4028/www.scientific. net/AMR.189-193.766
- 14. Pal, K., Bhattacharya, S., and Pal, S. K. 2010. Investigation on arc sound and metal transfer modes for on-line monitoring in pulsed gas metal arc welding. Journal of Materials Processing Technology 210: 1397-1410. DOI: 10.1016/j.jmatprotec.2010.03.029
- 15. Yamamoto, E., Yamazaki, K., Suzuki, K., and Koshiishi, F. 2010. Effect of flux ratio in flux-cored wire on wire melting behaviour and

- fume emission rate. Welding in the World 54: R154-R159. DOI: 10.1007/BF03263501
- 16. Song, G., Wang, P., and Liu, L. M. 2010. Study on AC-PMIG welding of AZ31B magnesium alloy. Science and Technology of Welding & Joining 15: 219-225. DOI: 10.1179/136217110X12665048207656
- 17. Era, T., Ueyama, T., and Hirata, Y. 2009. Spatter reduction in gas metal arc welding of stainless steel sheets using controlled bridge transfer process. Science and Technology of Welding & Joining 14: 708-716. DOI: 10.1179/136217109X12518083193595
- 18. Ersoy, U., Hu, S. J., and Kannatey-Asibu, E. 2008. Observation of arc start instability and spatter generation in GMAW. Welding Journal 87(2): 51-s to 56-s.
- 19. Shi, Y., Liu, X., Zhang, Y., and Johnson, M. 2008. Analysis of metal transfer and correlated influences in dual-bypass GMAW of aluminum. Welding Journal 87(9): 229-s to 236-s.
- 20. Cheng, Y., Yu, R., Zhou, Q., Chen, H., Yuan, W., and Zhang, Y. M. 2021. Real-time sensing of gas metal arc welding process: A literature review and analysis. Journal of Manufacturing Processes 70: 452-469. DOI: 10.1016/j.jmapro.2021.08.058
- 21. Jones, L. A., Eagar, T. W., and Lang, J. H. 1998. Magnetic forces acting on molten drops in gas metal arc welding. Journal of Physics D: Applied Physics 31: 93-106.
- 22. Planck, M. 1901. Ueber das Gesetz der Energieverteilung im Normalspectrum. Annalen der Physik 309. DOI: 10.1002/ andp.19013090310
- 23. Griem, H. R., and Barr, W. L. 2008. Spectral line broadening by plasmas. IEEE Transactions on Plasma Science 3. DOI: 10.1109/ TPS.1975.4316912
- 24. Zielinska, S., Pellerin, S., Dzierzega, K., Valensi, F., Musiol, K., and Briand, F. 2010. Measurement of atomic Stark parameters of many Mn I and Fe I spectral lines using GMAW process. Journal of Physics D: Applied Physics 43. DOI: 10.1088/0022-3727/43/43/434005
- 25. Omar, B. 2011. Spectral line broadening in dense plasmas. Journal of Atomic, Molecular, and Optical Physics 2011. DOI: 10.1155/2011/850807
- 26. Oks, E., ed. 2019. Stark broadening of spectral lines in plasmas. DOI: 10.3390/books978-3-03897-456-7
- 27. Karabourniotis, D., and Karras, C. 1985. Line broadening in optically thick gas discharges: Influence on plasma temperature determination. Journal of Applied Physics 57. DOI: 10.1063/1.335306
- 28. Bergman, T. L., Lavine, A. S., Incropera, F. P., and DeWitt, D. P. Fundamentals of Heat and Mass Transfer, 8th Edition. Wiley.
- 29. Gouffe, A. 1945. Corrections d'ouverture des corps-noirs artificels compte tenu des diffusions multiples internes. Revue d'Optique Théorique et Instrumentale 24: 1-10.
- 30. Schöpp, H., Sperl, A., Kozakov, R., Gött, G., Uhrlandt, D., and Wilhelm, G. 2012. Temperature and emissivity determination of liquid steel S235. Journal of Physics D: Applied Physics 45. DOI: 10.1088/0022-3727/45/23/235203
- 31. Goett, G., Kozakov, R., Uhrlandt, D., Schoepp, H., and Sperl, A. 2013. Emissivity and temperature determination on steel above the melting point. Welding in the World 57. DOI: 10.1007/s40194-013-0054-2
- 32. Touloukian, Y. S., Powell, R. W., Ho, C. Y., and Klemens, P. G. 1971. Thermophysical Properties of Matter: The TPRC Data.
- 33. Schmidt, E., and Eckert, E. 1935. Über die Richtungsverteilung der Wärmestrahlung von Oberflächen. Forschung auf dem Gebiet des Ingenieurwesens A 6. DOI: 10.1007/BF02578830
- 34. Del Campo, L., Pérez-Sáez, R. B., Esquisabel, X., Fernández, I., and Tello, M. J. 2006. New experimental device for infrared spectral directional emissivity measurements in a controlled environment. Review of Scientific Instruments 77. DOI: 10.1063/1.2393157

- 35. Siewert, E., Schein, J., and Forster, G. 2013. Determination of enthalpy, temperature, surface tension and geometry of the material transfer in PGMAW for the system argon-iron. Journal of Physics D: Applied Physics 46: 224008. DOI: 10.1088/0022-3727/46/22/224008
- 36. Okuno, T. 1985. Spectra of optical radiation from welding arcs. Industrial Health 23. DOI: 10.2486/indhealth.23.53
- 37. Zabirov, A. 2013. "Study of the explosion effect in electrode metal droplets of binary AlMg alloys in pulsed GMA welding." In Mathematical Modelling of Weld Phenomena, edited by Sommitsch, C., and Enzinger, N., Page, T., 95-107.
- 38. Kozakov, R., Gött, G., Schöpp, H., Uhrlandt, D., Schnick, M., Häßler, M., Füssel, U., and Rose, S. 2013. Spatial structure of the arc in a pulsed GMAW process. Journal of Physics D: Applied Physics 46: 224001. DOI: 10.1088/0022-3727/46/22/224001
- 39. Duke, D. J., Knast, T., Thethy, B., Gisler, L., and Edgington-Mitchell, D. 2019. A low-cost high-speed CMOS camera for scientific imaging. Measurement Science and Technology 30. DOI: 10.1088/1361-6501/ab1832
- 40. Choubey, B., Mughal, W., and Gouveiac, L. 2019. "CMOS circuits for high-performance imaging." In High Performance Silicon Imaging: Fundamentals and Applications of CMOS and CCD Sensors. DOI: 10.1016/B978-0-08-102434-8.00005-2
- 41. Vision Research. 2012. Phantom V210 / V310 / V12.1 / V710 color and spectral response curve.
- 42. Imaging Solutions GmbH. 2016. Spectral response curve IDT MotionProY4.
- 43. ISO. 2019. ISO 12232:2019. Photography Digital still cameras - Determination of exposure index, ISO speed ratings, standard output sensitivity, and recommended exposure index, p. 1–21.
- 44. Panasonic. Panasonic develops technology for highly sensitive image sensors using micro color splitters. Panasonic Newsroom Global.
- 45. Togashi, H., Yagi, I., Murata, M., Kuribayashi, M., Koga, F., Yamaguchi, T., Oike, Y., Ezaki, T., Hirayama, T., Watanabe, T., Joei, M., Hayashi, T., Hirata, S., Fukuoka, S., Ando, Y., Sato, Y., and Yamamoto, J. 2019. Three-layer stacked color image sensor with 2.0-μm pixel size using organic photoconductive film. Technical Digest - International Electron Devices Meeting (IEDM). DOI: 10.1109/ IEDM19573.2019.8993553
- 46. Wootton, C. 2016. A Practical Guide to Video and Audio Compression: From Sprockets and Rasters to Macro Blocks. Taylor and Francis Group.
- 47. Shimadzu. 2015. LAN-A-HV-E007: High-speed imaging of fuel injection in automotive engines. Retrieved from shimadzu.com/an/ sites/shimadzu.com.an/files/pim/pim_document_file/applications/ application_note/9969/jpi715003.pdf.
- 48. Kunkel, T., and Reinhard, E. 2010. A reassessment of the simultaneous dynamic range of the human visual system. Proceedings - APGV 2010: Symposium on Applied Perception in Graphics and Visualization. DOI: 10.1145/1836248.1836251
- 49. Xiris Inc. Xiris solutions for weld inspection and monitoring. Retrieved from xiris.com.
- 50. MeltTools. MeltTools welding cameras. Retrieved from metltools.com.
- 51. Mann, S., Lo, R. C. H., Ovtcharov, K., Gu, S., Dai, D., Ngan, C., and Ai, T. 2012. Realtime HDR video for eyetap wearable computers, FPGA-based seeing aids, and glasseyes (eyetaps). 25th IEEE Canadian Conference on Electrical and Computer Engineering (CCECE).
- 52. Jang, H., Bang, K., Jang, J., and Hwang, D. 2020. Dynamic range expansion using cumulative histogram learning for high dynamic range image generation. IEEE Access 8. DOI: 10.1109/ ACCESS, 2020, 2975857

- 53. Vision Research. 2012. EDR extreme dynamic range. Retrieved from phantomhighspeed.com/-/media/project/ameteksxa/visionresearch/documents/features/edr.pdf.
- 54. Kadoi, K., Fujinaga, A., Yamamoto, M., and Shinozaki, K. 2013. The effect of welding conditions on solidification cracking susceptibility of type 310S stainless steel during laser welding using an in-situ observation technique. Welding in the World 57. DOI: 10.1007/ s40194-013-0023-9
- 55. Shinozaki, K., Yamamoto, M., Kawasaki, A., Tamura, T., and Wen, P. 2008. Development of evaluation method for solidification cracking susceptibility of Inconel600/SUS347 dissimilar laser weld metal by in-situ observation. Materials Science Forum 580-582: 49-52. DOI: 10.4028/www.scientific.net/MSF.580-582.49
- 56. Hornberg, A. 2017. Handbook of Machine and Computer Vision. DOI: 10.1002/9783527413409
- 57. International Safety Equipment Association. 2020. ANSI/ISEA Z87.1:2020, American National Standard for occupational and educational personal eye and face protection devices.
- 58. Wilhelm, G., Gött, G., Schöpp, H., and Uhrlandt, D. 2010. Study of the welding gas influence on a controlled short-arc GMAW process by optical emission spectroscopy. Journal of Physics D: Applied Physics 43: 434004. DOI: 10.1088/0022-3727/43/43/434004
- 59. Wilhelm, G., Kozakov, R., Gött, G., Schöpp, H., and Uhrlandt, D. 2012. Behaviour of the iron vapour core in the arc of a controlled short-arc GMAW process with different shielding gases. Journal of Physics D: Applied Physics 45: 85202. DOI: 10.1088/0022-3727/45/8/085202
- 60. Zielińska, S., Musioł, K., Dzierżęga, K., Pellerin, S., Valensi, F., de Izarra, C., and Briand, F. 2007. Investigations of GMAW plasma by optical emission spectroscopy. Plasma Sources Science and Technology 16: 832-838. DOI: 10.1088/0963-0252/16/4/019
- 61. Dos Santos, E. B. F. 2017. Influence of current pulse profile on metal transfer in pulsed gas metal arc welding. Masters thesis, University of Waterloo.
- 62. Nomura, K., Kataoka, K., Mimura, K., Hirata, Y., and Kishi, T. 2016. Tomographic spectroscopic observation of argon and metal vapor behavior in MIG arc welding. Welding in the World 60. DOI: 10.1007/s40194-015-0267-7
- 63. ISO/IEC JTC 1/SC 29. 2020, Information technology Coding of audio-visual objects. Part 14: MP4 file format. ISO/IEC 14496-
- 64. ISO/IEC. 2017, Information technology High efficiency coding and media delivery in heterogeneous environments. Part 2: High efficiency video coding. ISO/IEC 23008-2:2017.
- 65. ITU-T. 2019, High efficiency video coding. Recommendation ITU-T H.265. ITU Telecommunication Standardization Sector.
- 66. ISO/IEC JTC 1/SC 29. 2021, Information technology Coded representation of immersive media. Part 3: Versatile video coding.
- 67. Bankovski, J., Koleszar, J., Quillio, L., Salonen, J., Wilkins, P., and Xu, Y. RFC 6386 - VP8 data format and decoding guide. Retrieved from tools.ietf.org/html/rfc6386.
- 68. Hunt, J. 2016. VP9 bitstream and decoding process specification v0.6. Google.
- 69. Alliance for Open Media. Release AV1 bitstream and decoding process specification (v1.0.0-errata1). Retrieved from github.com/ AOMediaCodec/av1-spec/releases/tag/v1.0.0-errata1.
- 70. ATSC. 2015. A/72 parts 1, 2, and 3. NextGen TV. Retrieved from atsc.org/atsc-documents/a72-parts-1-2-and-3/.
- 71. ETSI. 2019. Digital video broadcasting (DVB); specification for the use of video and audio coding in broadcast and broadband applications.

- 72. ITU. 2015. BT. 2020: Parameter values for ultra-high definition television systems for production and international programme exchange. Retrieved from itu.int/rec/R-REC-BT.2020/en.
- 73. DCI LLC. 2018. DCI digital cinema system specification, Version 1.3.
- 74. Society of Motion Picture and Television Engineers. 2015. SMPTE standard – Ultra high definition television – Image parameter values for program production. ST 2036-1:2014.
- 75. Society of Motion Picture and Television Engineers. 2008. SMPTE ST 274:2008 – Television – 1920 × 1080 image sample structure, digital representation and digital timing reference sequences for multiple picture rates. DOI: 10.5594/SMPTE.ST274.2008
- 76. Society of Motion Picture and Television Engineers. 2011. SMPTE ST 2048-2:2011 – 2048 \times 1080 digital cinematography production image FS/709 formatting for serial digital interface.
- 77. Society of Motion Picture and Television Engineers. 2019. SMPTE ST 2081-12:2019 – 4320-line and 2160-line source image and ancillary data mapping for quad-link 6G-SDI. DOI: 10.5594/ SMPTE.ST2081-12.2019
- 78. V.R. Inc, PCC Software. Retrived from phantomhighspeed.com/ resourcesandsupport/phantomresources/pccsoftware.
- 79. Adobe Premiere Pro. Retrieved from adobe.com/products/ premiere.html.
- 80. Lightworks: The professional editor for everyone. Retrieved from lwks.com.
 - 81. Final Cut Pro X Apple. Retrived from apple.com/ca/final-cut-pro.
- 82. DaVinci Resolve. Blackmagic Design. Retrieved from blackmagicdesign.com/ca/products/davinciresolve.
 - 83. Kdenlive | Libre Video Editor. Retrieved from kdenlive.org/en.
 - 84. OpenShot Video Editor. Retrieved from openshot.org/.
 - 85. Avidemux. Retrieved from avidemux.sourceforge.net.
- 86. HandBrake: Open Source Video Transcoder. Retrieved from handbrake.fr.

STUART DAN GUEST, GREGOR GÖTT, GOETZ DAPP, JULIEN CHAPUIS, and PATRICIO MENDEZ (pmendez@ ualberta.ca) are with the University of Alberta, Edmonton, Alberta, Canada